J Mater Sci

Materials for life sciences

Electrospun Mg/poly(lactic-co-glycolic acid) composite scaffold for urethral reconstruction

Liqu Huang[1,*], Xianli Wang[2,3], Yue Zhang[2,3], Zhaojun Cheng[2,3], Feng Xue[2,3], Yunfei Guo[1], Yongji Deng[1], Chenglin Chu[2,3], Li Tao[2,3,*], and Jing Bai[2,3,4,*]

[1] *Department of Urology, Children's Hospital of Nanjing Medical University, 72 Guangzhou Road, Nanjing 210008, Jiangsu, China*
[2] *School of Materials Science and Engineering, Southeast University, Jiangning, Nanjing 211189, Jiangsu, China*
[3] *Jiangsu Key Laboratory for Advanced Metallic Materials, Jiangning, Nanjing 211189, Jiangsu, China*
[4] *Institute of Medical Devices (Suzhou), Southeast University, Suzhou 215000, China*

Received: 9 February 2020
Accepted: 9 June 2020

ABSTRACT

Hypospadias is a common congenital malformation of the male urogenital system. As a recently arisen reconstruction method for hypospadias, polymer tissue engineering urethral scaffold often results in necrosis and other complications due to the lack of bioactivity. To improve the bioactivity of polymer, in this work, we prepared biodegradable Mg/poly(lactic-co-glycolic acid) (PLGA) composite nanofiber scaffolds by electrospun with 3, 6, and 9 wt.% of micron-scale Mg particles. The mechanical properties of the PLGA scaffold gradually decrease with the addition of Mg particles but still at an acceptable level. On the other hand, these composite scaffolds show very good biocompatibility and promotional bioactivity, namely non-cytotoxicity, gradual proliferation enhancement, and good adhesion state of human adipose stem cells (HADSCs) on the scaffold surface. Besides, through quantitative real-time polymerase chain reaction (qRT-PCR) test, different genes expression levels of human umbilical vein endothelial cells (HUVECs) were also gradually up-regulated with the increase in Mg content. The present results indicate that Mg containing PLGA scaffolds might not only have the potential to promote tissue regeneration related to urethral repair, but also stimulate endothelial cells to achieve vascularization and anti-inflammatory functions. Consequently, considering both the mechanical properties and bioactivity for clinical demand, the Mg/PLGA composite scaffolds with suitable Mg contents are promising for the regeneration of defective urethral tissues.

Liqu Huang and Xianli Wang have contributed equally to the work.

Address correspondence to E-mail: huanglq@njmu.edu.cn; tao@seu.edu.cn; baijing@seu.edu.cn

https://doi.org/10.1007/s10853-020-04951-6

Published online: 18 June 2020

Abbreviations

PLGA	Poly(lactic-co-glycolic acid)
HADSCs	Human adipose stem cells
HUVECs	Human umbilical vein endothelial cells
ECM	Extracellular matrix
SVR	Surface to volume ratio

Introduction

As a type of congenital malformation in the male genitourinary system, there is a high incidence, about 1/200–1/300, of hypospadias [1]. Especially for severe patients with obvious penile curvature and long urethral defects, surgical repair of hypospadias is difficult due to the lack of suitable urethroplasty materials, resulting in a very high incidence of surgical complications (45.7%) and the reoperation rate (24.5%), respectively [2, 3].

To developing promising materials and methods for the treatment of hypospadias, electrospinning technology, which was introduced into the biomedical field such as drug delivery systems, surgical masks, and medical dressings in the 1990s [4], has recently encouraged a new interest with the rise of tissue engineering. First, these reticular structures constructed by electrospinning nanofibers can mimic the properties of the extracellular matrix (ECM) and provide a three-dimensional porous structure with high porosity to enhance the interaction between the scaffold and cells [5]. Besides, in comparison with other methods like solvent casting, 3D printing, or wet-spinning, the electrospun nanofiber scaffold is much softer and more flexible, therefore easier to stick to the soft urethral tissue. In addition, these nanofibers, which have a high surface to volume ratio (SVR), are considered to be excellent drug carriers [6].

However, the common biomedical polymer for electrospinning, such as polylactic acid (PLA), polycaprolactone (PCL), and poly(lactic-co-glycolic acid) (PLGA) [7], is nearly biological inert and may not be able to provide optimum conditions for tissue healing [8]. To improve the bioactivity of these polymers, a good strategy is to introduce the foreign bioactive agent. For example, vascular endothelial growth factor and basic fibroblast growth factors could promote the generation of blood vessels and contribute to the survival of the graft [9]. On the other hand, these growth factors may fail to obtain a durable establishment of tissue blood supply between lesion site and scaffold because of unstable efficiency [10], which limits their application in tissue engineering.

Mg, as a typical biodegradable medical metal, is recently better known for its bioactivity, and could be an ideal substitute for the current bioactive agent. The Mg-enriched microenvironment was reported to have the function of promoting tissue remodeling, stimulating the osteogenic differentiation of stem cells [11], stimulating vascular endothelial cell proliferation, enhancing the mitogenic response to angiogenic factors, and attenuating the response to lipopolysaccharide (LPS) [12]. The bioactivity of Mg mainly comes from the Mg^{2+}, which is released during degradation through the chemical or electrochemical reaction between Mg and solution and, therefore, has a relative long-term release dynamics stage, especially when Mg is obstructed by the biodegradable polymer coating [13]. Moreover, Mg can also regulate the acidic products generated by the hydrolysis of biodegradable polymer because of its alkaline corrosion products, thus reducing the stimulation to tissues and the inflammation response [14]. Consequently, it is expected that there is a great clinical potential for the biodegradable polymer matrix composites functionally reinforced by Mg. Although there have been some works on the biodegradable Mg/polymer composites, for example, Adhikari et al. [15] so far reported the electrospun Mg/PCL electrospun nanofiber scaffolds and the potential application in tissue engineering recently. Their work well confirmed the feasibility of electrospun Mg/polymer scaffold in vivo, but for specific indications, there is still a lack of systematic microstructural and biological evaluation.

For the treatment of hypospadias, it has been proved that the induction of adipose stem cells into endothelial cells has the function of promoting angiogenesis in vivo and has been widely used in the treatment of ischemic diseases and other research fields [16]. The combination of stem cell vascularization and appropriate active drugs to construct a highly vascularized tissue-engineered urethra in vitro plays a critical role in the survival of the graft after urethral reconstruction [17].

Therefore, in this paper, to study the effect of the addition of Mg into polymer scaffold on the urethral related cells, we fabricated three kinds of Mg/PLGA composite nanofiber scaffold with 3, 6 and 9 wt.% Mg

particles added by electrospinning. Micron-scale Mg particles were used as a bioactive-reinforced phase and PLGA 50:50 was used as a matrix based on the considerations of the moldability, mechanical properties, and degradation period. The microstructures, biocompatibility, and biological response to human adipose stem cells (HADSCs) and human umbilical vein endothelial cells (HUVECs) were also studied. It is expected to provide some theoretical support for the future application of a biologically active urethral scaffold.

Materials and methods

Materials

PLGA (lactide: glycolide = 50:50, M_w = 100 kDa, ρ = 1.34 g·cm^{-3}) (Jinan Daigang Biomaterial Co., Ltd. China) and pure Mg powders (ρ = 1.74 g·cm^{-3}, Tangshan Weihao Mg powder Co. Ltd. China) were selected as raw materials to prepare the experimental composite scaffold. Some chemical reagents, like 1,1,1,3,3,3-hexafluoro-2-propanol (HFIP) (Aladdin Biochemical Technology Co., Ltd., China) and phosphate-buffered saline (PBS,0.01 M) (Biosharp Co. Ltd., China), were used during preparation and testing process. For biological evaluations, Cell Counting Kit-8 (CCK-8) was obtained from Beyotime (China) and Dulbecco's modified Eagle's medium (DMEM), fetal bovine serum (FBS), penicillin and streptomycin (PS), LIVE/DEAD^{TM} Viability/Cytotoxicity Kit, Alexa Fluor^{TM} 594 Phalloidin, DAPI (4′,6-diamidino-2-phenylindole), and TRIZOL agent were purchased from Thermo Fisher Scientific US.

Preparation of Mg/PLGA nanofiber scaffold by electrospinning

To prepare the Mg/PLGA scaffolds with three different contents of Mg particles (3, 6, 9 wt.%, corresponding to the code of NS-3, NS-6, and NS-9 in this paper, respectively), Mg powders were first dissolved into 10 mL HFIP solution until even by magnetic stirring for 2 h. After that, 1.5 g PLGA 50:50 was then added into the blended suspension and magnetically stirred overnight at room temperature. Subsequently, the blended suspension was poured into 5.0 ml-plastic syringes equipped by the electrospinning machine (Beijing Yongkangleye Technology co., Ltd. ET-2, China). The syringe with a needle of 23G-diameter was propelled at a rate of 18 μL/min and moved back and forth at a speed of 0.1 m/s. The distance of the needle to the collector platform was 15 cm with an applied voltage of 12 kV. After electrospinning, these scaffolds were dried in a vacuum oven to remove the residual solvent and stored in a drying dish to prevent degradation. The thickness of the scaffolds before peeling off from the aluminum foil was determined by an Eddy current thickness gauge (CT 800, Huasheng Instrument Research Institute, Shenyang, China) with a resolution of 1 μm. In this study, the thickness of the scaffold prepared by 10 ml suspension was about 200 ± 30 μm.

Physicochemical characterization

Microstructures

Micro-morphologies of Mg powders particles and scaffolds were observed by Sirion 200 Field Emission Scanning Electron Microscope (SEM) at a voltage of 15 kV. To observe Mg particles, 0.1 g Mg powders were dissolved in 10 mL absolute ethanol and vibrated by ultrasound for 1 min, and then one drop of the suspension was dropped on the conductive copper tape and dried for 30 min to remove the residual ethanol. To observe scaffolds by SEM, samples before and after degradation were first sputter-coated with a thin gold layer. The size of Mg particles, the diameter of nanofibers, and pore size (diameter of inscribed circle) are obtained based on the mean value of 300 statistics using Nano Measurer v.1.2.5. The composition and distribution of Mg particles in scaffolds were detected by energy-dispersive spectrometer (EDS) equipped by SEM. The porosity and density of the nanofiber scaffolds were calculated as follows [18]:

$$\text{Apparent density (g/cm}^3\text{)} = \frac{\text{mass of scaffold (g)}}{\text{scaffold thickness (cm)} \times \text{scaffold area (cm}^2\text{)}} \quad (1)$$

$$\text{Porosity}(\%) = \left(1 - \frac{\text{apparent density}(\text{g}\cdot\text{cm}^{-3})}{\text{PLGA or PLGA/Mg bulk density}(\text{g/cm}^3)}\right) \times 100 \quad (2)$$

$$\text{PLGA or PLGA/Mg bulk density}(g \cdot cm^{-3}) = \frac{1}{\left(\frac{w_1}{d_1} + \frac{w_2}{d_2}\right)} \quad (3)$$

where w_1 and w_2 are weight fractions, d_1 and d_2 are the density of PLGA and Mg, respectively. The thickness of the scaffold is the average value of 16 points (the center of each part after being equally divided into 16 equal parts).

XRD and ATR-FTIR analysis

X-ray diffractometer ((XRD, Bruker, D8-discover) with Cu Kβ radiation (45 kV, 40 mA) was used to detect the crystallographic structure of Mg powders and scaffolds over diffraction angles (2θ) of 10°–90° at a scanning speed of 0.15 s/step. The chemical structure of the scaffolds was confirmed through an ATR-FTIR spectrum (Nicolet iS10, Thermo Scientific, USA) in the range of 4000–500 cm^{-1}. Water contact angle measurements were taken at room temperature by an OCA15pro instrument (Data Physics, Germany) with a droplet of 0.5 μl.

Determination of mechanical properties

The tensile strength, elastic modulus, and elongation of the scaffolds were tested using CMT 4503 universal testing machine (SANS, China) with a load cell of 100 N at a crosshead speed of 5 mm/min under the guidance of ASTM D882-02. Both ends of the scaffolds were pasted with double-sided adhesive tape to prevent the clamp from slipping.

In vitro biological evaluations

First, the prepared scaffolds were cut into circles with a diameter of 1.5 cm and then were irradiated under ultraviolet light (λ = 250 nm) for 24 h followed by soaked in 75% ethanol for 3 h. Second, using sterile conditions, the scaffolds were gently washed with phosphate buffer saline (PBS, pH 7.4) three times and moved into a new plate with a pair of sterilized tweezers. Third, HADSCs and HUVECs, after the third passage from the primary cells, were plated directly on the scaffolds in the 24-well cell culture plate with a cell density of 5×10^3 cells/well and 10^4 cells/well, respectively. Then they were immersed in DMEM (Gibco, Thermo Fisher Scientific) containing 0.2% FBS (Atlanta Biologicals, Lawrenceville, GA). The culture medium was changed every 2 days. To keep the scaffold from floating, a homemade iron ring after sterilized was used to hold it (Supplementary Information Figure S1). All operations were performed in a biological safety cabinet. At last, the cell culture plates were kept in a humidified incubator (5% CO_2, 37 °C, Thermo Fisher Scientific).

Cytocompatibility and cytotoxicity

HADSCs were cultured on the surface of the scaffolds to determine the growth and cytocompatibility, and the CCK-8 test was performed to determine the cytotoxicity of the composite scaffolds. The cells after cultured for 1,4 and 7 days were stained with LIVE/DEAD™ reagent. To observe staining images, Laser Confocal Microscope (Zeiss, LSM700) was used to photograph the distribution of dead (red) and living (green) cells on the scaffolds. Image J software was employed to count the number of living cells on the scaffold per area. The CCK-8 solution (10% in α-MEM) was added in each well, and then the medium was incubated at 37 °C in 5% CO_2 for 3 h to detect the cytotoxicity of the scaffold material after co-cultured with HADSCs for 1,4,7 days. Cells incubated only in the DMEM with 0.2% FBS without co-cultured with scaffold were used as the control group. The absorbance value of the culture medium was detected by the enzyme marker at λ = 450 nm. The viability compared to the control group was calculated through the equation below:

$$\text{Viability}\ (\%) = \frac{OD_i}{OD_c} \times 100\% \quad (4)$$

where OD_i and OD_c are the optical density (OD) value of the supernatant of the experimental groups and the control group, respectively.

Cell morphology and adherence

Fluorescence staining and SEM were performed to assess the cytoskeletal structure of adherent cells. First, HADSCs were seeded on the prepared scaffolds and allowed to grow for 7 days. Afterward, the scaffolds with the adhered cells were collected and washed with PBS three times. Then the samples were fixed with 4% paraformaldehyde, the cytoskeletons and the nucleus were stained with Alexa Fluor™ 594 Phalloidin and DAPI in PBS, respectively, for 15 min.

After that, the samples were washed with PBS three times to remove the unbound dyes and then mounted with Vectashield mounting medium. Then the cell morphological images were observed under a Laser Confocal Microscope. Next, the specimens after fixed with 4% paraformaldehyde were dried naturally and sputter-coated with a thin gold layer for SEM observation.

Assessment of gene expression

The biological properties of the composite scaffolds were further evaluated by quantitative Real-Time polymerase chain reaction (qRT-PCR) to measure the relative mRNA levels of endothelial cells. HUVECs were inoculated on the scaffolds and incubated on 24-well plates with a density of around 1×10^4 cells/well in each well and incubated with serum-free (0.2% FBS) media for 24 h before the experiment. Afterward, the scaffolds with cells were washed gently by PBS for three times. Then 0.25 mL Trizol reagent was added into each well and pipetted several times until the cells and the scaffolds were dissolved. Next, 0.2 mL of chloroform was added into a tube with 1 ml of chloroform added and then the tube was shaken before centrifuging for 15 min (4 °C, 12,000 rpm). After that, the upper liquid with 0.5 ml of isopropyl alcohol added was centrifuged again for 10 min (4 °C, 12,000 rpm) and the supernatant was discarded. Followed by adding 1 ml of DEPC water into the tube and centrifuging again for 5 min (4 °C, 7500 rpm). Then the white precipitate at the bottom of the tube is the total RNA extracted after discarding the supernatant. 20 μl of RNase-free DEPC water was added to the centrifuge tube and then incubated at 55–60 °C for 10 min to dissolve the RNA for further experiments [19]. The qRT-PCR test was performed by using an ABI 7500 Sequencing detection system (Thermo Fisher Scientific) according to the manufactures' guidance. Levels of fibroblast growth factor 1 (FGF1), vascular endothelial growth factor (VEGF), vascular endothelial growth factor receptor 1 (FLT1/VEGFR1), fibronectin 1 (FN1), nitric oxide synthase 3 (NOS3), angiotensin II receptor type 1 (AGTR1), C–C motif chemokine ligand 2 (CCL2), vascular cell adhesion molecule 1 (VCAM1) were quantified. HUVECs incubated only in DMEM with serum-free (0.2% FBS) media were set as the control group. The primer sequences used are shown in Supplementary Information Table 1. The mRNA levels were normalized to β-actin mRNA.

In vitro degradation test

To evaluate whether the Mg particles would fall off from the scaffold, NS-9 was selected for the in vitro degradation experiment. Scaffold pieces were cut into squares (1×1 cm^2) followed by irradiating under ultraviolet light ($\lambda = 250$ nm) for 24 h. After that, each piece was placed into a centrifuge tube containing 10 ml of PBS (pH 7.4). Then the tubes were sealed up and put on a shaker at 37 °C. After 7-day degradation, all the samples were taken out, rinsed in distilled water, and dried for SEM observation.

Statistical analysis

SPSS Statistics 22.0 software (SPSS, Inc., Chicago, IL, USA) was used to conduct statistical analyses. All experimental data were expressed as mean ± standard deviation (SD) of 3 to 5 measurements. "One way ANOVA" was performed to statistical analysis followed by post hoc LSD-tests. Significant difference was considered if the p was below 0.05.

Results

Electrospun PLGA and Mg/PLGA nanofiber scaffolds with a percentage of less than 10 wt.% were successfully fabricated, and the physicochemical and biological properties of those scaffolds were compared to assess its availability as a potential scaffold for soft tissue repairing application. The electrospinning process of the Mg/PLGA composite scaffold is shown in Fig. 1a. Since the magnesium particles were deposited in the rotating collector, some were embedded in the fibers while others directly exposed on the surface of the scaffolds (Fig. 1b), while the diameter of the fibers in the scaffold did not change much with the increase in Mg content (Supplementary Information Figure S2).

Physicochemical characterization

Characterizations of Mg powders received

Figure 2a shows that the as-received Mg powders are mainly spheroidal particles with an average diameter of 14.5 ± 5.4 μm (Fig. 2b). EDS results illustrate that

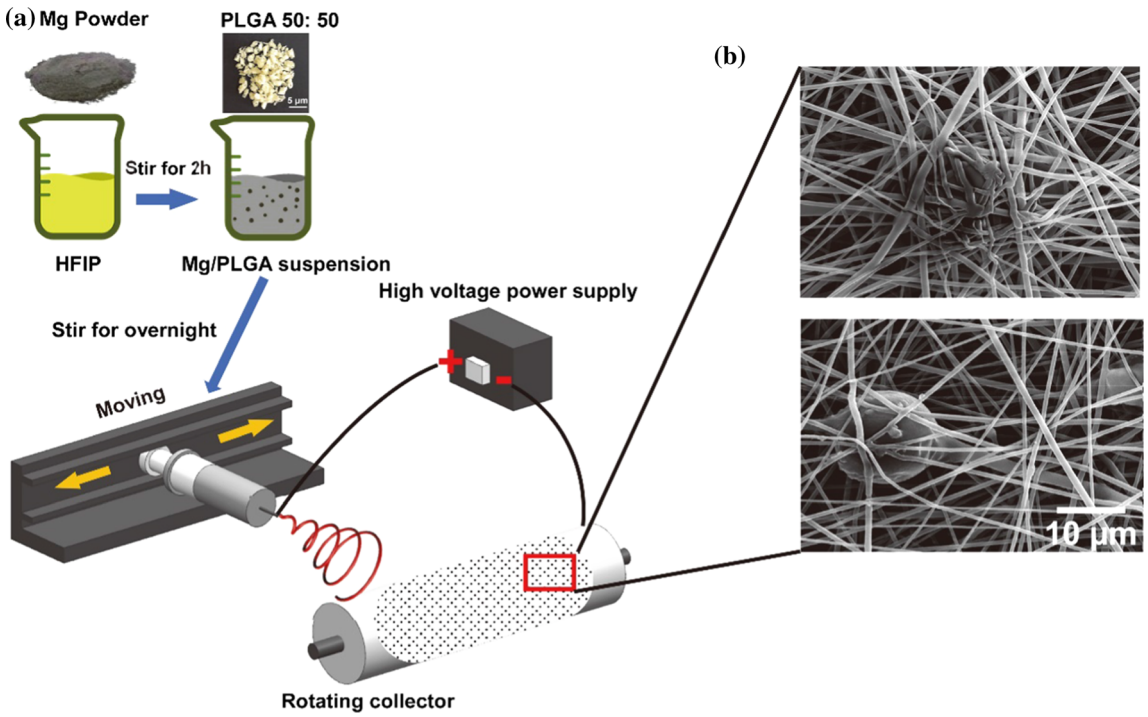

Figure 1 The preparation process of the Mg/PLGA nanofiber scaffold by electrospinning. This illustration shows how the Mg/PLGA suspension mixture was prepared and how the nanofibers deposited on the rotating collector (**a**). Nanofiber scaffolds after fabrication were cut and observed by SEM (**b**). During the fiber deposition process, the collector rotated and the cylinder shifted back and forth, which made Mg particles deposit uniformly.

the compositions of the Mg powder are mainly Mg close to 98% and a small amount of Cu and O (Fig. 2c). These O atoms were introduced probably due to the inevitable oxidization of Mg powder in the process of atomization and storage. There were only the diffraction peaks corresponding to Mg detected (PDF No.35-0821) in the XRD pattern (Fig. 2d) without any MgO peak, indicating the relative amount of MgO is extremely little.

Microstructural analysis

The morphology and distribution of Mg particles on the surface of the experimental scaffolds can be observed from their SEM images and corresponding EDS Mapping of Mg element, as shown in Fig. 3a and b, where these Mg particles appear to be a relatively uniform distribution in all specimens without obvious agglomeration. The good dispersion ability of Mg particles is attributed to the moving needle on the rotating collector as well as the electrostatic attractions and repulsions caused by the high pressure (Fig. 1) [20]. The micro-morphologies of PLGA nanofibers and Mg particles with higher magnification can be seen from Fig. 1b, where these nanofibers oriented randomly with uniform diameter and the Mg particles are covered by a thin polymer film on the surface. Measurement results show that the porosity and pore size of these scaffolds decrease with the increase in Mg contents from 65.4% and 4.2 ± 1.2 μm to 56.4% and 3.2 ± 0.8 μm, respectively (Fig. 3c and refer to Supplementary Information Table 2). The reason is probably that some of the positions of pores are occupied by the Mg filler (Fig. 1b).

XRD and ATR-FTIR analysis

Figure 4a shows the XRD patterns of nanofiber scaffolds with the different Mg content. There are almost no crystallization peaks in the PLGA scaffold due to the amorphous structure of PLGA50:50. The relative intensity of Mg peaks gradually increases but without peak shift with Mg content rising from 3 wt.% to 9 wt.%, which indicates the Mg particles had been compounded on the fibers without changing the structure of Mg. Besides, no obvious diffraction peaks of MgO were observed on the composite scaffold. It

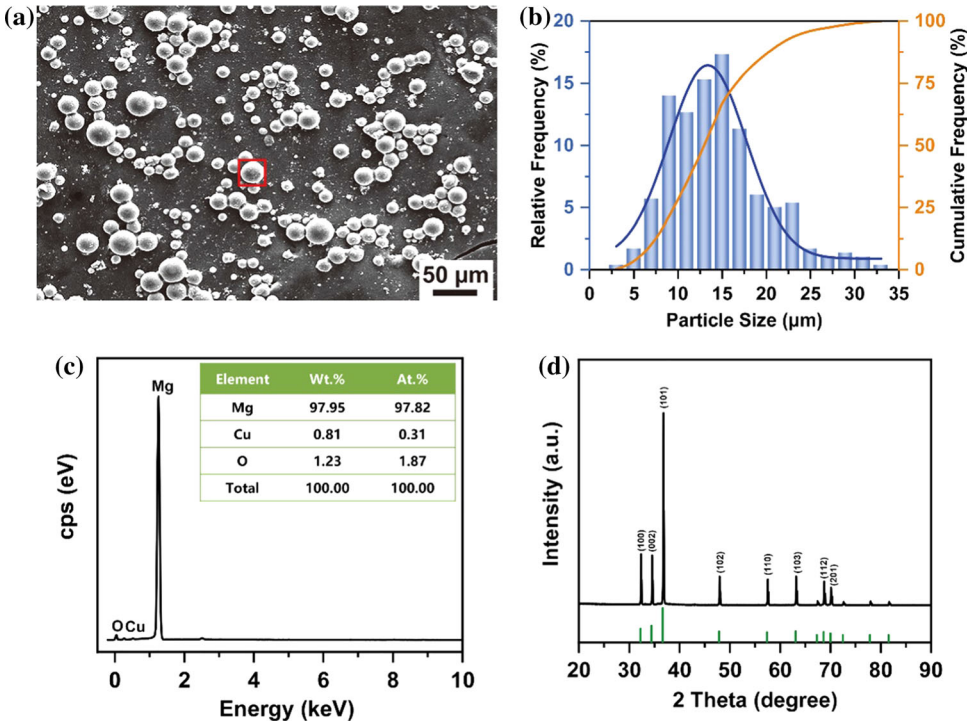

Figure 2 Characterizations of the as-received Mg particles by **a** SEM, **b** Size distribution calculation, **c** EDS composition analysis, and **d** XRD crystal structure detection.

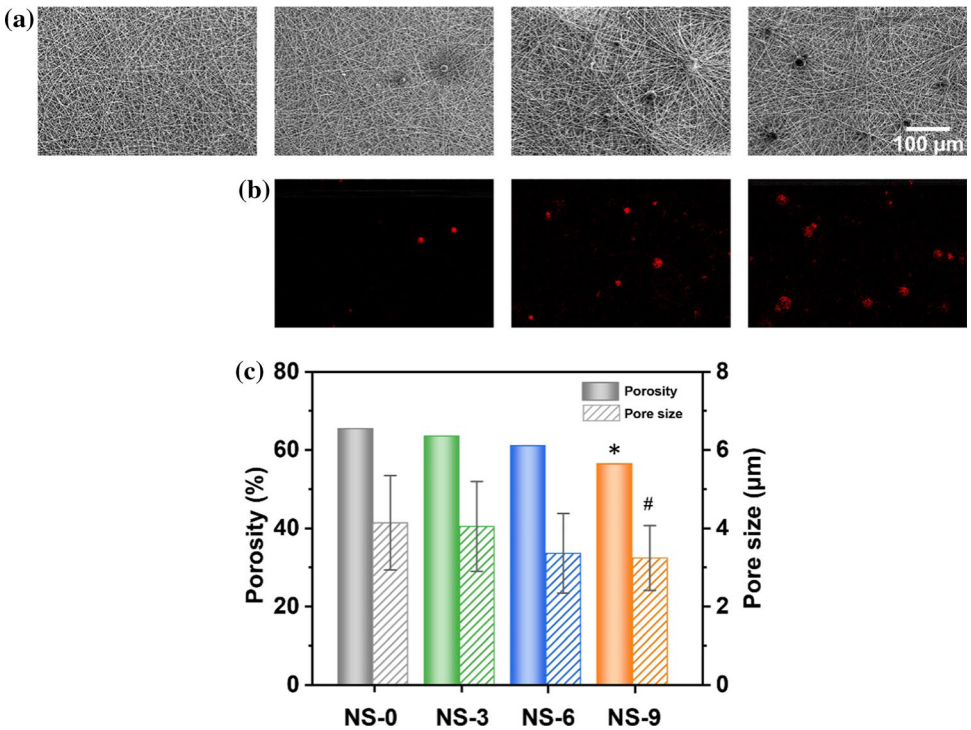

Figure 3 Microstructures of the prepared PLGA and Mg/PLGA scaffolds detected by **a** SEM under lower magnification. **b** EDS mapping distribution. **c** Porosity and pore size of the prepared PLGA and Mg/PLGA scaffolds calculated by Nano Measurer 1.2.5. ($n = 5$ in each group; *$p < 0.05$; #p < 0.05. * and # indicate that the values are significantly different from the NS-0 group).

suggests that the thin polymer film covered on the Mg particles effectively prevented the Mg powder from being oxidized during electrospinning at elevated temperature. From Fig. 4b, typical absorption bands observed at 1754 cm^{-1},1711 cm^{-1}, 1091 cm^{-1}, 2948 cm^{-1}, and 2849 cm^{-1} correspond to the stretching vibration peak of the C = O in the ester, stretching vibration peak of the C-O, asymmetric stretching vibration peaks of the C–O–C, asymmetric stretching vibration peaks of CH_2, respectively. By

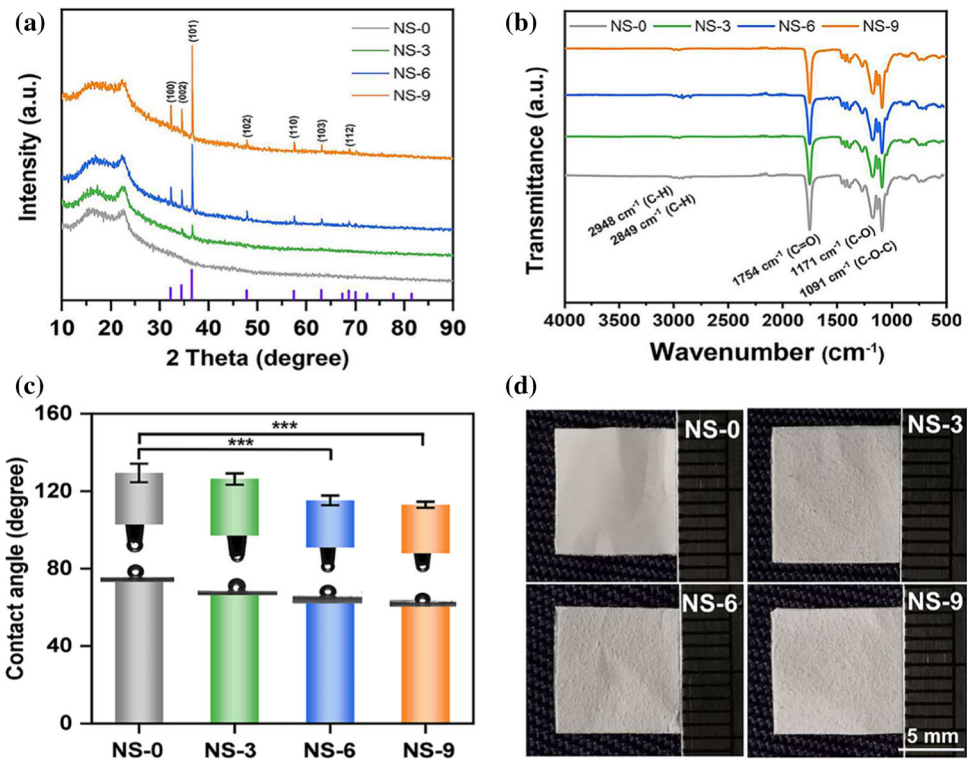

Figure 4 The prepared PLGA and Mg/PLGA scaffolds detected by **a** XRD crystal structure analysis and **b** ATR-FTIR spectrum for functional groups, **c** water contact angle test for hydrophilicity, and **d** stereoscopic microscope observation for apparent morphology.

comparing the characteristic peak intensity and peak position of the four scaffolds, it can be seen that the chemical structure of the scaffold matrix did not change with the addition of Mg particles or the action of high voltage [21].

Hydrophilic test

Figure 4c presents that with the increase in Mg content to 9 wt.%, there is a continuous reduction in water contact angle value of the nanofiber scaffolds from 129.4 ± 4.7° to 113.1 ± 1.6°. It is a result of the presence of hydrophilic Mg powder with hydroxyl groups attached to the surface and the increased surface fluctuation of the scaffold (Fig. 4d). Generally, a scaffold is more conducive for cell adhesion and growth if the hydrophilicity of the scaffold is better [22].

Mechanical properties

The typical stress–strain curves in Fig. 5a show the mechanical properties of the nanofiber scaffolds, including tensile strength and elongation, reduces gradually due to the introduction of Mg particles, from ~ 9.3 MPa and 380% for NS-0 to ~ 5.3 MPa and 250% for NS-9 (Fig. 5b). It is because micron-scale Mg could not be effectively wrapped inside the PLGA fibers, resulting in many macroscopic defects in scaffolds. Meanwhile, Mg particles hinder the entanglement among fibers, bringing about the weakening of interactions among polymer macromolecules and the fast disintegration of fibers. Although there is a decrease in the mechanical properties when Mg particles were added, for clinical application, scaffold with an elongation over 200% is enough to adhere to the soft tissue tightly. More Mg contents up to 15% and 20% will lead to a more serious deterioration in the mechanical properties (refer to Supplementary Information Fig. 3 and Table 3).

In vitro biological tests

Cytocompatibility and cytotoxicity

Figure 6a shows the number of living cells on the scaffold increased and even occupied the whole vision via time. Cell counting results (Fig. 6b) indicate cell densities of all scaffolds after 4 days and 7 days are significantly higher than that of the first day. It is noted that there is a burst of cell proliferation of NS-9 on the 7th day, suggesting the scaffold with 9 wt.% Mg powers addition is particularly

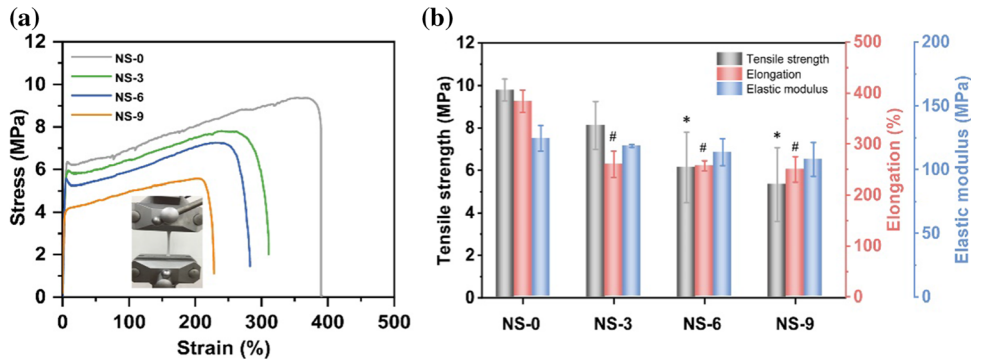

Figure 5 Mechanical properties of the prepared PLGA and Mg/PLGA scaffolds tested by tensile experiments. **a** Stress–strain curves. **b** Tensile strength, elongation, and elastic modulus. (n = 5 in each group; $*p < 0.05$; $\#p < 0.05$. * and # indicate that the values are significantly different from the NS-0 group).

favored for the growth of HADSCs. The cytotoxicity test result by CCK-8 kit manifests the relative cell viability of all scaffolds are over 80% on the first day, compared with the control group (Fig. 6c), presenting toxicity of Grade I [23]. As culture time went by, the viability of cells rose further. Thus, PLGA and Mg particles after the electrospinning process are not only non-toxic but also suitable for the growth of HADSCs.

Cell morphology and adherence

Cell morphologies and adhesion, as well as cell interactions with nanofibers, are included in cellular compatibility which was observed via Laser Confocal Microscope and SEM. The nucleus staining on the 7th day (Fig. 7a) shows the nucleus spread throughout the whole vision and the cells proliferate well on the scaffolds. It is consistent with the result of cell proliferation. It was also observed that typical spindle-shaped on the scaffolds and their cytoskeleton are complete, which reveals the introduction of Mg does not damage the normal cytoskeleton of cells. Figure 7b shows that cells attach well and spread along nanofibers, even extending into the interstitial space of the scaffolds after 7 days. Cell spreading and extension on the nanofibers is probably aided by the fact that the fibers were submicron in size and thinner than the size of the cells, as been reported for other fibers [24] (Supplementary Information Figure A). Moreover, a large number of adipose stem cells grow into the pores of the scaffolds, and the proliferation of cells on NS-9 was fastest and even join together into sheets. It means that more Mg provides a better condition for cell growth compared with other groups, and the increased hydrophilicity of scaffolds by the addition of Mg fillers might also account for it.

Gene expression analysis

The gene expression level under the influence of Mg in HUVECs cultured on the prepared scaffolds for 24 h was detected by qRT-PCR. In comparison with the control group, the FGF1, VEGF, FLT1/VEGFR1, FN1, NOS3, AGTR1, CCL2 and VCAM1 gene expression of HUVECs treated with composite scaffolds increase with Mg content rising. For the NS-9 group, these eight genes are up-regulated to 1.6–5.1 folds, unequally (Fig. 8). Most of the investigated genes are related to neovascularization and the HUVECs adhesion signaling pathways [25]. Higher genes level means that Mg stimulated endothelial cell behaviors, such as cell adhesion and growth of fresh blood vessels [26], which is consistent with our expectations of rapid tissue growth and angiogenesis at the lesion site.

Discussions

This paper aims to construct cell–scaffold complexes as precursors to repair defective urethral tissues. Induced differentiation of HADSCs into endothelial cells is one of the methods to generate vascularized tissue. It has been proved to have the function of promoting angiogenesis in vivo and also widely used in the treatment of ischemic diseases [16]. Hence, HADSCs were chosen to co-culture with the Mg/PLGA composite scaffolds. HUVECs, as a type of endothelial cells, were selected to verify the

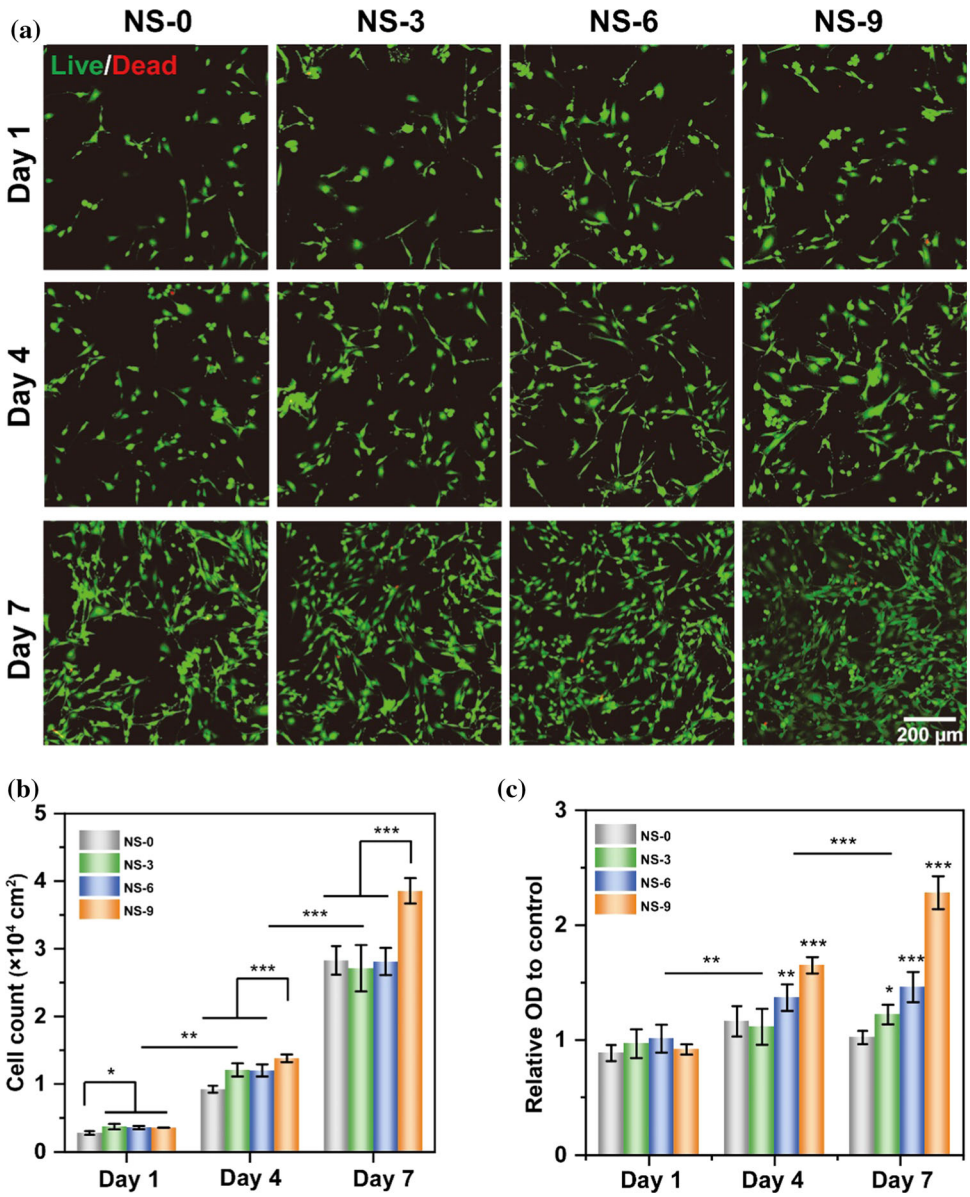

Figure 6 Biocompatibility and cytotoxicity tests of HADSCs co-cultured with the prepared PLGA and Mg/PLGA scaffolds for 1,4, 7 days detected by **a** Laser Confocal Microscope with fluorescence staining of dead and living cells, **b** living cell counting. **c** CCK-8 test for cell toxicity. ($n = 3$ in each group; *$p < 0.05$; **$p < 0.01$; ***$p < 0.001$. *above the error bar indicates that the value is significantly different from the control).

expression level of angiogenesis and anti-inflammation relative genes under the function of Mg powders. Therefore, to construct a highly vascularized tissue-engineered urethra in vitro, the combination of stem cell vascularization technology and appropriate active drug (Mg) is the key to solve the problem of graft survival after urethral reconstruction.

In our experiment, to improve the dispersion uniformity of Mg particles in the matrix, the following measures were taken: (1) Mg powders were mixed with the organic solvent and mechanically stirred before PLGA was added. (2) We strictly controlled the absolute content of Mg to avoid powders agglomeration and blockage of needles. (3) We replaced the syringes and needles every 2 h, and the mixture was kept stirring before being pumped into the syringe. (4) The electrospinning machine we used has the function of carrying the needle to move back and forth, which greatly enhances the dispersion.

Spherical Mg particles were added into the PLGA to increase its biological activity (Fig. 2a). Previous reports have shown that spherical particles, compared with irregular ones, showed a slower degradation rate due to the smaller SVR, when Mg was included in a PLA/Mg composite material [27]. Hence, spherical Mg particles are more suitable than irregular particles to maintain the concentration of Mg^{2+} around the damaged tissue at a certain level for

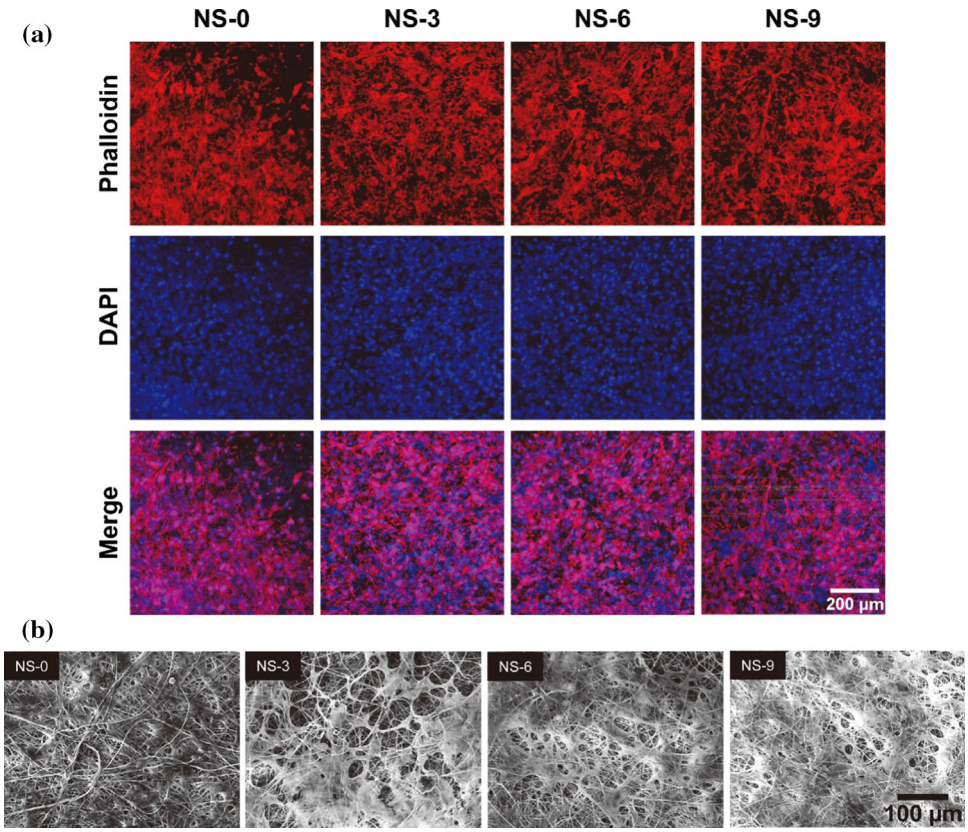

Figure 7 The cytoskeletons and nucleus images of the HADSCs co-cultured with the prepared PLGA and Mg/PLGA scaffolds for 7 days observed by **a** Laser Confocal Microscope. HADSCs adhesion states on the prepared PLGA and Mg/PLGA scaffolds observed by **b** SEM.

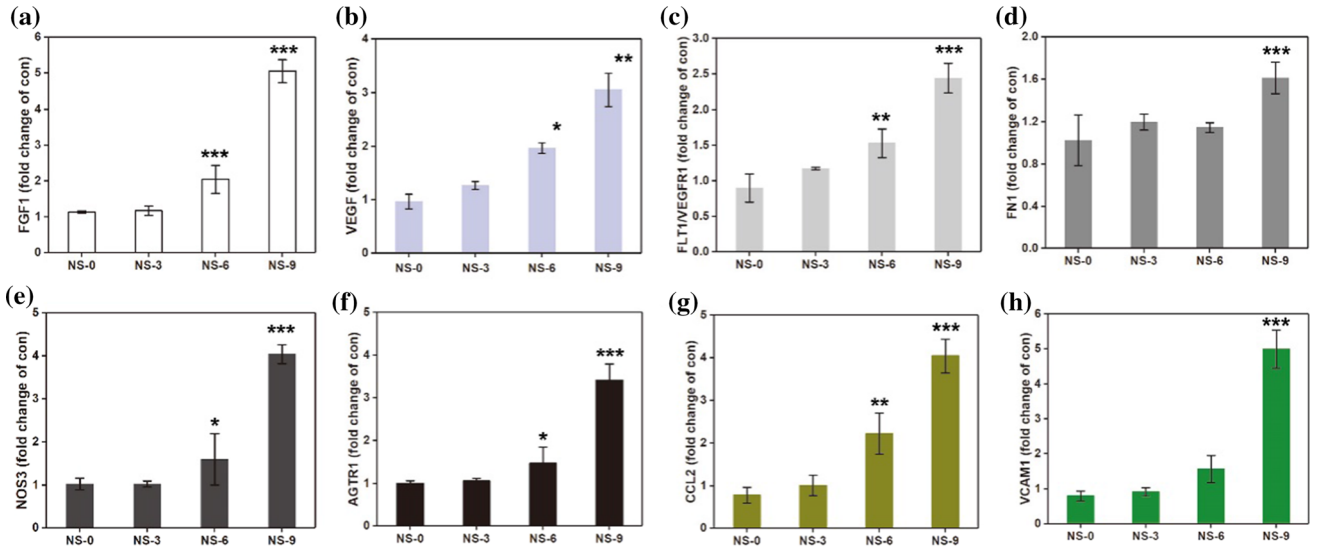

Figure 8 The gene expression trend of HUVECs after culture on the prepared PLGA and Mg/PLGA scaffolds for 24 h detected by qRT-PCR. **a** FGF1, **b** VEGF, **c** FLT1/VEGFR1, **d** FN1, **e** NOS3, **f** AGTR1, **g** CCL2, and **h** VCAM1. ($n = 3$ in each group; $^{*}p < 0.05$; $^{**}p < 0.01$; $^{***}p < 0.001$. *Above the error bar indicates that the value is significantly different from the control).

a longer time. During electrospinning, Mg particles deposit on the nanofibers layer by layer, so some particles are tightly wrapped by nanofibers and the others are exposed to the surface. Even in the latter case, the particle is still wrapped by a thin layer of the polymer film (Fig. 1b). Once the scaffold is immersed in the body fluids, the Mg particles are gradually corroded instead of falling off from the matrix. Two

factors may account for it: (1) Water molecules can penetrate the polymer fiber and react with magnesium; (2) the corrosion rate of magnesium is significantly higher than that of PLGA. So, we can observe that the Mg particle has corroded and leaves an empty polymer shell before the polymer fibers break (Fig. 9a) and the others tightly wrapped in the nanofibers remain (Fig. 9b).

The loose and porous 3D structure constructed by electrospinning simulates the structure of ECM which consists of a cross-linked network of proteins and glycosaminoglycans. Besides, the porous structure was conducive to the oxygen supply and prompt discharge of the metabolic waste of cells, which ensures the smooth flow of nutrients needed for cell growth within the scaffold. [28]. However, if the porosity and pore size was much less than 33.5% and 6 μm, respectively, the small pore may hinder stem cell infiltration, cell–scaffold interactions, and tissue growth [29]. In our experiment, the porosity of the scaffold is as low as 56.4% after 9 wt% Mg was added (Fig. 3c). It is because the porous structure is blocked by the aggregated Mg particles and fibers (Fig. 1b). Therefore, the content of Mg fillers in the scaffold should be controlled in terms of promoting cell metabolism.

Although the hydrophilicity of the nanofiber scaffold prepared by electrospinning is not as good as we expected, the addition of Mg particles properly makes up for this deficiency. Micron-scale Mg particles with larger surface energy tended to adsorb some functional groups with high activity in the air, such as hydroxyl groups, thus reducing the hydrophobicity of the scaffold (Fig. 4c) and promoting the adhesion of cells [30]. However, because the amount of Mg added was little and the particles were covered by thin polymer films, the hydrophilicity of the composite scaffolds did not improve much. So, the detection of hydroxyl groups was not obvious (Fig. 4b).

One of the basic mechanical properties of soft tissue scaffolds is they are flexible enough to fit tightly to the lesion site for muscular movements [31]. However, as a repair membrane for urethral wounds, the nanofiber scaffold is not load-bearing, as long as it has sufficient toughness to closely fit the wound surface without rupture during the suturing. It can be found from Fig. 5a that all the scaffolds undergo significant strengthening stages before breaking. Compared with polymer film fabricated by solvent casting with less than 10% elongation [32], the elongation of PLGA is closed to 400%, which effectively prevents the scaffold from breaking during suturing. Moreover, the strength of the stretched scaffold continues to increase before breaking (Fig. 5a). That because once nanofibers were under tension, polymer macromolecular chains in the amorphous region tended to overcome the secondary valence bonds among long molecular chains and further stretched and oriented, until the major valence bond broke and the fibers disintegrated [33]. However, Mg particles weakened the secondary valence bond between the fiber macromolecules, as well as acted as stress concentration centers to prevent the effective transfer of stress from the polymer matrix [34]. Hence, increasing amounts of Mg results in the decrease in elongation and strength of the composite scaffolds. Consequently, Mg content in the scaffold should also be controlled to fit the desired mechanical properties.

Biocompatibility, cell proliferation, and adhesion on scaffold materials are the preconditions for a scaffold to be used as tissue engineering precursors. The increased cell viability of HADSCs and low cytotoxicity of Mg/PLGA composite scaffolds via time indicate good biocompatibility (Fig. 6a–c). The good cell proliferation state and increased cell

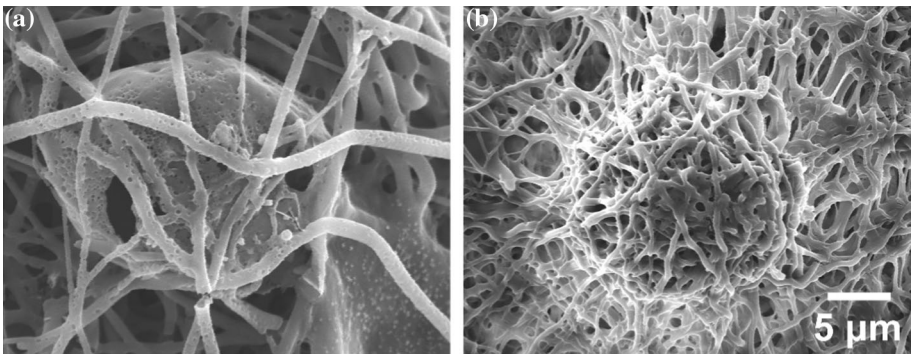

Figure 9 Representative SEM microstructures of NS-9 nanofiber scaffold after immersed in PBS for 7 days. **a** Mg particle exposed on the surface of the scaffold was preferentially corroded and only a thin shell was left. **b** Mg particle was wrapped by nanofibers.

density of HADSCs on Mg/PLGA scaffolds might be attributed to the appropriate rate and amount releasing of Mg^{2+} [35]. Moreover, MMP2 up-regulated by an effective concentration of Mg^{2+} has previously been shown to enhance cell proliferation on the ECM [36]. Furthermore, HADSCs showed increased stretching (Fig. 7a) and a tendency to grow into the pores of scaffolds (Fig. 7b), which demonstrates that the composite scaffolds are qualified as tissue engineering carriers. And increased irregularity in height of the surface (Fig. 4d) also contributes to the better adhesion of HADSCs on the scaffolds. These observations demonstrate the HADSCs, once seeded on scaffolds, can quickly climb up into pieces and have the potential to form whole tissues. If stem cells are induced to differentiate into endothelial cells during cell seeding, we believe that a combination of cells and the composite scaffold, especially for NS-9, has the potential to accelerate tissue healing.

Additionally, a developed vascular network is also vital for the integration of artificial scaffold and original human tissue. Summarizing the qRT-PCR array data, it can be found that seven genes were markedly upregulated in HUVECS by Mg-containing scaffolds, including FGF1, FLT1/VEGFR1, VEGF, NOS3, AGTR1, CCL2, and VCAM1. As for the involved genes, their expression levels rise in a dose-dependent manner with magnesium (Fig. 8). This is because the concentration of Mg^{2+} released from the composite scaffold (less than 30 mg/L) is much lower than the critical concentration (about 10 mM) under which the expression of these genes was inhibited [25]. Therein, the FGF1 gene is widely recognized to have a significant effect on cell adhesion and tissue healing, which is the most highly up-regulated by NS-9 of all the genes studied (5.1-fold). Also, VEGF (3.1-fold by NS-9) signaling plays a major role in promoting the proliferation and differentiation of the endothelial lineage from the earliest stages of development via activation of the VEGF Receptor (2.4 ± 0.2 fold by NS-9). And it stimulates platelet activation, thus promoting endothelial cell migration, proliferation, and angiogenesis [37]. FN1 (1.6-fold by NS-9) has been verified to be equipped with the function of re-endothelialization and a significant reduction in neointimal formation. So, it is often used in a gene-eluting stent [38]. NOS3 (4.0-fold by NS-9), as an angiogenesis regulator, was confirmed to lead to enhanced production of NO and further increase cell migration ability [39]. The expression level change of VCAM1 (4.1-fold) and CCL2 (5.0-fold) indicates that strong inflammatory chemokines are regulated once the Mg reach at 9 wt.% [40]. Therefore, we believe that the composite scaffold has the potential to activate the behaviors of HUVECs and thus can promote neovascularization in the scaffold-endothelial cells complexes. Furthermore, the present findings strongly support the possibility of using Mg/PLGA scaffolds with moderate Mg fillers content for the treatment of hypospadias. Among them, 9 wt.% is a better choice compared with those with few additions (Refer to Supplementary Information Table 4).

Nanofillers, such as MgO [41], ZnO [42], TiO_2 [43], hydroxyapatite [44], and europium hydroxide [34], have already been investigated on their potential to induce stem cell differentiation or enhance endothelial cells proliferation. Compared with those fillers, Mg has its incomparable advantages including full degradability and alkaline corrosion products which is the bane of Escherichia coli, Staphylococcus aureus, and other bacteria [45]. Moreover, Mg, a reactive metal, reacts violently with body fluids and releases hydrogen gas which may combine with water to form hydrogenated water. It is a powerful antioxidant and has been found to have beneficial effects in some preclinical disease models such as controlling the rate of cognitive decline [46, 47]. But this beneficial effect can be only achieved when the implants in the body produce hydrogen slowly and in small amounts. It is because the rapid degradation of Mg creates gas-filled cavities that could exert stress and damage to adjacent tissues [48]. The preparation of electrospun scaffolds by mixing Mg particles with polycaprolactone had already been reported recently [15]. In the present study, the content of Mg particles in the polymer was cut down and thus resulted in the reduction of hydrogen production, as well as the improvement of the mechanical strength and elongation of nanofiber scaffolds. As tissue-engineered scaffolds, it is necessary to balance their biological and physical properties to achieve a better treatment effect. The addition of Mg particles to the matrix leads to a continuous decrease in the mechanical properties and 15 wt.% of Mg addition in the scaffold can quickly result in the fast fracture of the composite scaffold (Supplementary Information Figure S3). Besides, lower porosity and smaller pore size may not be appropriate for a cell to grow into the scaffold. Hence, there is a proper range to the amount of filler added to the scaffold in terms of balancing physical and biological properties. Thus, on

the condition of meeting the biological function requirement, the addition of Mg should be as less as possible. In total, these findings support the use of Mg as bioactive medicine in scaffolds in the treatment of urethral defect disease, and 9 wt.% Mg/PLGA is a good alternative.

In this study, the effects of Mg particles in the Mg/PLGA scaffolds on HADSCs and HUVECs were investigated systematically, and the results demonstrated the composite scaffolds have very good mechanical and biological properties. Furthermore, we would like to induce adipose stem cells into endothelial cells to construct an artificial urethra repair material with bionic structure and pre-angiogenesis function and in vivo experiments will also be conducted.

Conclusions

In our work, Mg/PLGA composite scaffolds with 3–9 wt.% Mg particle addition were successfully fabricated by electrospinning for urethral tissue engineering applications. The mechanical properties of the PLGA scaffold gradually decrease with the addition of Mg particles but still at an acceptable level. On the other hand, the composite scaffolds not only showed improved hydrophilicity but also presented non-cytotoxicity, good cell adhesion state, and gradual proliferation enhancement of HADSCs on the scaffold surface with Mg content increasing. Based on the results of qRT-PCR on HUVECs, it is also confirmed that the composite scaffold possessed the possibility of application in terms of their activating endothelial cells' behaviors including cell adhesion, angiogenesis, anti-inflammatory response, and platelet activation on ischemic tissue by up-regulating the expression of the related genes. In short, the studies on Mg/PLGA composite scaffolds show that the scaffold with 9 wt.% Mg particles has the best comprehensive properties, including good flexibility and bioactivity, among all experimental materials. Thus, the developed Mg/PLGA composite scaffold in this study will be a promising implant for patients with hypospadias.

Acknowledgements

Jing Bai acknowledges the support from the National Natural Science Foundation of China (51971062) and the Science and Technology Project of Jiangsu Province (BE2019679). Liqu Huang, Jing Bai, Yunfei Guo, and Li Tao acknowledge the support from Fundamental Research Funds for the Central Universities (2242018K3DN02). The authors thank Leiying Miao (Nanjing Stomatological Hospital, Medical School of Nanjing University) for the help in sample preparation.

Compliance with ethical standards

Conflict of interest The authors declare that they have no conflict of interest.

Electronic supplementary material: The online version of this article (https://doi.org/10.1007/s10853-020-04951-6) contains supplementary material, which is available to authorized users.

References

[1] Baskin LS, Ebbers MB (2006) Hypospadias: anatomy, etiology, and technique. J Pediatr Surg 41:463–472. https://doi.org/10.1016/j.jpedsurg.2005.11.059

[2] Huang L, Guo Y, Ge Z, Lu R, Deng Y, Ma G, Chen F (2017) A new modification of the Duckett technique for one-stage repairing urethral plate transected hypospadias: another option for severe hypospadias? Int Urol Nephrol 49:2091–2097. https://doi.org/10.1007/s11255-017-1690-z

[3] Castagnetti M, El-Ghoneimi A (2010) Surgical management of primary severe hypospadias in children: systematic 20-year review. J Urol. 184:1469–1475. https://doi.org/10.1016/j.juro.2010.06.044

[4] Wang G, Yu D, Kelkar AD, Zhang L (2017) Electrospun nanofiber: emerging reinforcing filler in polymer matrix composite materials. Prog Polym Sci 75:73–107. https://doi.org/10.1016/j.progpolymsci.2017.08.002

[5] Wang X, Ding B, Li B (2013) Biomimetic electrospun nanofibrous structures for tissue engineering. Mater Today 16:229–241. https://doi.org/10.1016/j.mattod.2013.06.005

[6] Li M, Guo Y, Wei Y, MacDiarmid AG, Lelkes PI (2006) Electrospinning polyaniline-contained gelatin nanofibers for tissue engineering applications. Biomaterials 27:2705–2715. https://doi.org/10.1016/j.biomaterials.2005.11.037

[7] De Filippo RE, Kornitzer BS, Yoo JJ, Atala A (2015) Penile urethra replacement with autologous cell-seeded tubularized collagen matrices. J Tissue Eng Regen M. 9:257–264. https://doi.org/10.1002/term.1647

[8] Ji W, Yang F, Seyednejad H, Chen Z, Hennink WE, Anderson JM, van den Beucken JJJP, Jansen JA (2012)

Biocompatibility and degradation characteristics of PLGA-based electrospun nanofibrous scaffolds with nanoapatite incorporation. Biomaterials 33:6604–6614. https://doi.org/10.1016/j.biomaterials.2012.06.018

[9] Zha Y, Lin T, Li Y, Zhang X, Wang Z, Li Z, Ye Y, Wang B, Zhang S, Wang J (2020) Exosome-mimetics as an engineered gene-activated matrix induces in situ vascularized osteogenesis. Biomaterials 247:119985. https://doi.org/10.1016/j.biomaterials.2020.119985

[10] Hiesinger W, Brukman MJ, McCormick RC, Fitzpatrick JR, Frederick JR, Yang EC, Muenzer JR, Marotta NA, Berry MF, Atluri P, Woo YJ (2012) Myocardial tissue elastic properties determined by atomic force microscopy after stromal cell-derived factor 1α angiogenic therapy for acute myocardial infarction in a murine model. J Thoracic Cardiovascul Surg. 143:962–966. https://doi.org/10.1016/j.jtcvs.2011.12.028

[11] Lin S, Yang G, Jiang F, Zhou M, Yin S, Tang Y, Tang T, Zhang Z, Zhang W, Jiang X (2019) A magnesium-enriched 3D culture system that mimics the bone development microenvironment for vascularized bone regeneration. ADV SCI. 6:1900209. https://doi.org/10.1002/advs.201900209

[12] Maier JAM, Bernardini D, Rayssiguier Y, Mazur A (2004) High concentrations of magnesium modulate vascular endothelial cell behaviour in vitro. Molecul Basis Dis. 1689:6–12. https://doi.org/10.1016/s0925-4439(04)00025-0

[13] Cai H, Meng J, Li X, Xue F, Chu C, Guo C, Bai J (2019) In vitro degradation behavior of Mg wire/poly(lactic acid) composite rods prepared by hot pressing and hot drawing. Acta Biomater 98:125–141. https://doi.org/10.1016/j.actbio.2019.05.059

[14] Rezwan K, Chen QZ, Blaker JJ, Boccaccini AR (2006) Biodegradable and bioactive porous polymer/inorganic composite scaffolds for bone tissue engineering. Biomaterials 27:3413–3431. https://doi.org/10.1016/j.biomaterials.2006.01.039

[15] Adhikari U, An X, Rijal N, Hopkins T, Khanal S, Chavez T, Tatu R, Sankar J, Little KJ, Hom DB, Bhattarai N, Pixley SK (2019) Embedding magnesium metallic particles in polycaprolactone nanofiber mesh improves applicability for biomedical applications. Acta Biomater 98:215–234. https://doi.org/10.1016/j.actbio.2019.04.061

[16] Sinha Ray S (2012) Polylactide-based bionanocomposites: a promising class of hybrid materials. Account Chem Res. 45:1710–1720. https://doi.org/10.1021/ie302359x

[17] Chen K, Wu H, Chang C (2012) Tissue-engineered constructs for urethral regeneration. Urol Sci. 23:42–44. https://doi.org/10.1016/j.urols.2012.04.003

[18] Chong EJ, Phan TT, Lim IJ, Zhang YZ, Bay BH, Ramakrishna S, Lim CT (2007) Evaluation of electrospun PCL/gelatin nanofibrous scaffold for wound healing and layered dermal reconstitution. Acta Biomater 3:321–330. https://doi.org/10.1039/c1ee02201f

[19] Tsai W, Chen C, Chen J, Chang K (2006) The effects of types of degradable polymers on porcine chondrocyte adhesion, proliferation and gene expression. J Mater Sci Mater Med 17:337–343. https://doi.org/10.1007/s10856-006-8234-x

[20] Suryavanshi A, Khanna K, Sindhu KR, Bellare J, Srivastava R (2017) Magnesium oxide nanoparticle-loaded polycaprolactone composite electrospun fiber scaffolds for bone-soft tissue engineering applications: in vitro and in vivo evaluation. Biomed Mater 12:55011. https://doi.org/10.1088/1748-605x/aa792b

[21] Lin M, Firoozi N, Tsai C, Wallace MB, Kang Y (2019) 3D-printed flexible polymer stents for potential applications in inoperable esophageal malignancies. Acta Biomater 83:119–129. https://doi.org/10.1016/j.actbio.2018.10.035

[22] Dai J, Yang S, Jin J, Li G (2016) Electrospinning of PLA/-pearl powder nanofibrous scaffold for bone tissue engineering. RSC Adv. 6:106798–106805. https://doi.org/10.1039/c6ra21796f

[23] Wang J, Witte F, Xi T, Zheng Y, Yang K, Yang Y, Zhao D, Meng J, Li Y, Li W, Chan K, Qin L (2015) Recommendation for modifying current cytotoxicity testing standards for biodegradable magnesium-based materials. Acta Biomater 21:237–249. https://doi.org/10.1016/j.actbio.2015.04.011

[24] Pegg DE (1999) Principles of tissue engineering. Cryobiology 39:378–379. https://doi.org/10.1006/cryo.1999.2214

[25] Zhao N, Zhu D (2015) Endothelial responses of magnesium and other alloying elements in magnesium-based stent materials. Metallomics. 7:118–128. https://doi.org/10.1039/c4mt00244j

[26] Salajegheh A (2016) Vascular endothelial growth factor (VEGF). https://doi.org/10.1007/978-3-319-28140-7_58

[27] Zhao C, Wu H, Ni J, Zhang S, Zhang X (2017) Development of PLA/Mg composite for orthopedic implant: tunable degradation and enhanced mineralization. Compos Sci Technol. 147:8–15. https://doi.org/10.1016/j.compscitech.2017.04.037

[28] Xu C, Inai R, Kotaki M, Ramakrishna S (2004) Electrospun nanofiber fabrication as synthetic extracellular matrix and its potential for vascular tissue engineering. Tissue Eng A. 10:1160–1168. https://doi.org/10.1089/ten.2004.10.1160

[29] Aghajanpoor M, Hashemi-Najafabadi S, Baghaban-Eslaminejad M, Bagheri F, Mohammad MS, Azam SF (2017) The effect of increasing the pore size of nanofibrous scaffolds on the osteogenic cell culture using a combination of sacrificial agent electrospinning and ultrasonication. J Biomed Mater Res A. 105:1887–1899. https://doi.org/10.1089/ten.2004.10.1160

[30] Augustine R, Saha A, Jayachandran VP, Thomas S, Kalarikkal N (2015) Dose-Dependent effects of gamma irradiation on the materials properties and cell proliferation of electrospun polycaprolactone tissue engineering scaffolds. Int J Polym Mater Po. 64:526–533. https://doi.org/10.1080/00914037.2014.977900

[31] Dhal J, Fielding G, Bose S, Bandyopadhyay A (2012) Understanding bioactivity and polarizability of hydroxyapatite doped with tungsten. J Biomed Mater Res B Appl Biomater 100B:1836–1845. https://doi.org/10.1002/jbm.b.32751

[32] Khamsarn T, Supthanyakul R, Matsumoto M, Chirachanchai S (2017) PLA with high elongation induced by multi-branched poly(ethylene imine) (mPEI) containing poly(l-lactic acid) (PLLA) terminals. Polymer 112:87–91. https://doi.org/10.1016/j.polymer.2016.08.038

[33] Sinha-Ray S, Khansari S, Yarin AL, Pourdeyhimi B (2012) Effect of chemical and physical cross-linking on tensile characteristics of solution-blown soy protein nanofiber mats. Ind Eng Chem Res 51:15109–15121. https://doi.org/10.1021/ie302359x

[34] Augustine R, Nethi SK, Kalarikkal N, Thomas S, Patra CR (2017) Electrospun polycaprolactone (PCL) scaffolds embedded with europium hydroxide nanorods (EHNs) with enhanced vascularization and cell proliferation for tissue engineering applications. J Mater Chem B. https://doi.org/10.1039/c7tb00518k

[35] Yoshizawa S, Brown A, Barchowsky A, Sfeir C (2014) Magnesium ion stimulation of bone marrow stromal cells enhances osteogenic activity, simulating the effect of magnesium alloy degradation. Acta Biomater 10:2834–2842. https://doi.org/10.1016/j.actbio.2014.02.002

[36] Ries C, Egea V, Karow M, Kolb H, Jochum M, Neth P (2007) MMP-2, MTI-MMP, and TMP-2 are essential for the invasive capacity of human mesenchymal stem cells: differential regulation by inflammatory cytokines. Blood 109:4055–4063. https://doi.org/10.1182/blood-2006-10-051060

[37] Endo A, Nagashima K, Kurose H, Mochizuki S, Matsuda M, Mochizuki N (2002) Sphingosine 1-phosphate induces membrane ruffling and increases motility of human umbilical vein endothelial cells via vascular endothelial growth factor receptor and crkii. J Biol Chem 277:23747–23754. https://doi.org/10.1074/jbc.m111794200

[38] O'Brien B, Zafar H, Ibrahim A, Zafar J, Sharif F (2016) Coronary stent materials and coatings: a technology and performance update. Ann Biomed Eng 44:523–535. https://doi.org/10.1007/s10439-015-1380-x

[39] Dimmeler S, Dernbach E, Zeiher AM (2000) Phosphorylation of the endothelial nitric oxide synthase at ser-1177 is required for VEGF-induced endothelial cell migration. FEBS Lett 477:258–262. https://doi.org/10.1016/s0014-5793(00)01657-4

[40] Rochelson B, Dowling O, Schwartz N, Metz CN (2007) Magnesium sulfate suppresses inflammatory responses by human umbilical vein endothelial cells (HuVECs) through the NFκB pathway. J Reprod Immunol 73:101–107. https://doi.org/10.1016/j.jri.2006.06.004

[41] Roh H, Lee C, Hwang Y, Kook M, Yang S, Lee D, Kim B (2017) Addition of MgO nanoparticles and plasma surface treatment of three-dimensional printed polycaprolactone/hydroxyapatite scaffolds for improving bone regeneration. Mater Sci Eng, C 74:525–535. https://doi.org/10.1016/j.msec.2016.12.054

[42] Barui AK, Veeriah V, Mukherjee S, Manna J, Patel AK, Patra S, Pal K, Murali S, Rana RK, Chatterjee S, Patra CR (2012) Zinc oxide nanoflowers make new blood vessels. Nanoscale. 4:7861–7869. https://doi.org/10.1039/c2nr32369a

[43] Liu W, Su P, Chen S, Wang N, Webster TJ (2015) Antibacterial and osteogenic stem cell differentiation properties of photoinduced TiO_2 nanoparticle-decorated TiO_2 nanotubes. Nanomedicine-UK 10:713–723. https://doi.org/10.2217/nnm.14.183

[44] Culpepper Bonnie K, Morris David S, Prevelige Peter E, Bellis Susan L (2013) Engineering nanocages with polyglutamate domains for coupling to hydroxyapatite biomaterials and allograft bone. Biomaterials 34(10):2455–2462

[45] Robinson DA, Griffith RW, Shechtman D, Evans RB, Conzemius MG (2010) In vitro antibacterial properties of magnesium metal against *Escherichia coli*, Pseudomonas aeruginosa and Staphylococcus aureus. Acta Biomater 6:1869–1877. https://doi.org/10.1016/j.actbio.2009.10.007

[46] Ohsawa I, Ishikawa M, Takahashi K, Watanabe M, Nishimaki K, Yamagata K, Katsura K, Katayama Y, Asoh S, Ohta S (2007) Hydrogen acts as a therapeutic antioxidant by selectively reducing cytotoxic oxygen radicals. Nat Med 13:688–694. https://doi.org/10.1038/nm1577

[47] Hou C, Peng Y, Qin C, Fan F, Liu J, Long J (2018) Hydrogen-rich water improves cognitive impairment gender-dependently in APP/PS1 mice without affecting Aβ clearance. Free Rad Res SFRR Asia 52:1311–1322. https://doi.org/10.1080/10715762.2018.1460749

[48] Noviana D, Paramitha D, Ulum MF, Hermawan H (2016) The effect of hydrogen gas evolution of magnesium implant on the postimplantation mortality of rats. J Orthop Transl. 5:9–15. https://doi.org/10.1016/j.jot.2015.08.003